Inclusion of Rational Models in an Electromagnetic Transients Program: Y-Parameters, Z-Parameters, S-Parameters, Transfer Functions

Bjørn Gustavsen, *Senior Member, IEEE*, and H. M. Jeewantha De Silva

***Abstract*—Frequency-dependent effects in power system components and subnetworks can be efficiently represented via rational function-based models that characterize the component port behavior as a function of frequency. The port behavior can be defined by alternative parameter sets (e.g., admittance (Y-), impedance (Z-), or scattering (S-) parameters). The model extraction procedure approximates the port characteristics over a desired band of frequencies via a compact rational model. This paper shows a detailed procedure for interfacing such models with electromagnetic transients simulators via a Norton equivalent and convolution, for multiport Y-, Z- and S-parameter-based models. The interface of a multiport transfer function element is also shown. The procedure is applicable for models on pole-residue and state-space form. The correctness of these model implementations is demonstrated for a small electrical circuit. Application examples are shown for subnetwork modeling from computed Y-parameters and for cable modeling from measured S-parameters.**

***Index Terms*—Admittance parameters, companion model, convolution, Electromagnetic Transients Program (EMTP), impedance parameters, rational model, scattering parameters, simulation, transfer function.**

I. Introduction

RATIONAL models are useful for representing linear components with frequency-dependent behavior. In this paper, we focus on terminal modeling where we model the component's behavior with respect to a set of external ports (terminals). Typical applications include high-frequency representation of power transformers from frequency sweep measurements [1], [2] and wideband representation of subnetworks from frequency sweep computations[3]–[7], so-called frequency-dependent network equivalents (FDNEs).

The port behavior can be conveniently characterized by the admittance matrix $\mathbf{Y}$ or impedance matrix $\mathbf{Z}$, which defines the relation between voltages and currents at the ports. Techniques are available for calculating rational function approximants which accurately reproduce the port characteristics over a desired band of frequency while satisfying the physical requirements of symmetry, causality, stability, and passivity [8]–[15]. Another way of characterizing the port behavior is by incident and reflected waves which are related via the scattering parameter matrix $\mathbf{S}$ [20], [21]. The latter characterization is often preferred in high-speed electronics modeling over the admittance formulation due to more accurate measurements at very high frequencies. In addition to Y-, Z- and S-parameter models, which interact with the adjacent circuit over their ports, it is often useful to apply pure transfer functions models in a simulation. Such transfer function capability provides an easy way of observing internal voltages and currents in a subnetwork represented by a Y-, Z- or S-parameter-based port equivalent, and it reduces the computational burden of the model identification process as the number of ports is reduced.

Y-parameter-based rational models can be interfaced with Electromagnetic Transients Program (EMTP)-type tools via an equivalent circuit [3], [17]. The circuit equivalent option is, however, prone to accuracy problems and should therefore be avoided [29]. A better alternative would be to represent the model using convolutions [5], [18], [19], which is the standard way of representing frequency-dependent transmission lines [24]. However, most EMTP-tools do not offer such capability for interfacing user-provided models. As for S-parameter models, no EMTP-type tool has an interfacing capability in place. Here, one would have to convert the data into Y-parameters prior to model extraction. Such conversion may, however, seriously impair the quality of the final model.

In this paper, we show a unified procedure for including rational models in EMTP-type simulation programs using a convolution-based Norton equivalent for admittance, impedance, and scattering parameter-based models, and for transfer functions. We start by defining the alternative parameter definitions and physicality constraints and outline the appropriate procedures for creating rational-function-based models on pole-residue and state-space form. We describe, in detail, procedures for interfacing these models in an EMTP-type simulation environment based on trapezoidal integration and a fixed time step length with consideration to computational efficiency. After validating these implementations on a common example, we demonstrate the application of the interfacing capability on some relevant examples from subnetwork modeling and cable modeling.

Manuscript received September 11, 2012; revised December 21, 2012; accepted February 10, 2013. Date of publication March 15, 2013; date of current version March 21, 2013. This work was supported in part by the KPN project "Electromagnetic transients in future power systems," financed in part by the Research Council of Norway and in part by Dong Energy, EdF, EirGrid, Hafslund, National Grid, Nexans, RTE, Siemens WP, Statnett, Statkraft, and Vestas WS. Paper no. TPWRD-00943-2012.

B. Gustavsen is with SINTEF Energy Research, Trondheim N-7465, Norway (e-mail: bjorn.gustavsen@sintef.no).

H. M. J. De Silva is with the Manitoba Hydro International, Winnipeg, MB R3P 1A3, Canada (e-mail: jeewantha@hvdc.ca).

Color versions of one or more of the figures in this paper are available online at http://ieeexplore.ieee.org.

Digital Object Identifier 10.1109/TPWRD.2013.2247067

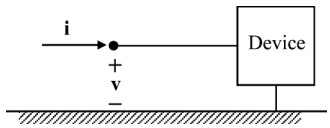

Fig. 1. n-port device with port voltages and currents.

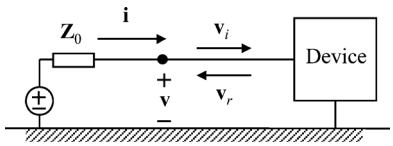

Fig. 2. n-port device with incident and reflected port waves.

In denoting variables and parameters, we have adopted the following notation: Bold uppercase: matrix; bold lowercase: vector; nonbold: scalar.

II. System Representations

A. Admittance $(Y-)$ and Impedance $(Z-)$ Parameters

We consider the modeling of an n-port device. The relation between voltage $\mathbf{v}$ and current $\mathbf{i}$ at the ports is in the s-domain given via the admittance matrix $\mathbf{Y}$ by (1) (See Fig. 1.) $\mathbf{v}$ and $\mathbf{i}$ are complex-valued vectors of length n while $\mathbf{Y}$ is a symmetrical, complex-valued matrix of dimension $n \times n$. Alternatively, the port behavior can be characterized by the impedance matrix $\mathbf{Z}$ (2), which is the inverse of $\mathbf{Y}$

$$\mathbf{i} = \mathbf{Y}\,\mathbf{v} \tag{1}$$

$$\mathbf{v} = \mathbf{Z}\,\mathbf{i}. \tag{2}$$

B. Scattering $(S-)$ Parameters

S-parameters characterize the relation between incident and reflected waves at the device ports when terminated by reference impedances. (See Fig. 2.) Typically, 50-Ω or 75-Ω reference impedances are used, matching the characteristic impedance of common measurement cables.

At the ports, we have relations (3)–(5) where subscripts i and r denote the incident and reflected wave, respectively. $\mathbf{Z}_0$ is a diagonal matrix whose jth entry holds the reference impedance at the jth port

$$\mathbf{v} = \mathbf{v}_i + \mathbf{v}_r \tag{3}$$

$$\mathbf{i} = \mathbf{i}_i - \mathbf{i}_r \tag{4}$$

$$\mathbf{i} = \mathbf{Z}_0^{-1}(\mathbf{v}_i - \mathbf{v}_r). \tag{5}$$

Inserting (3) and (5) into (1) gives the relation (6) between the reflected $(\mathbf{v}_r)$ and incident $(\mathbf{v}_\mathrm{i})$ voltage waves via the scattering matrix $\tilde{\mathbf{S}}$, where $\mathbf{I}$ is the identity matrix

$$\mathbf{v}_r = (\mathbf{I} + \mathbf{Z}_0\mathbf{Y})^{-1}(\mathbf{I} - \mathbf{Z}_0\mathbf{Y})\mathbf{v}_i = \tilde{\mathbf{S}}\,\mathbf{v}_i. \tag{6}$$

Equation (6) shows that the scattering parameters are dependent on the chosen reference resistors. It is common practice to normalize the voltage waves by dividing with the square root of the reference impedance. As a result, the square of the waves $\mathbf{v}_i$ and $\mathbf{v}_r$ gets dimension power and the associated waves $\mathbf{a}$ and $\mathbf{b}$ are accordingly termed power waves. Re-derivation of (6) with inclusion of the scaling gives the final result

$$\mathbf{b} = \mathbf{S}\,\mathbf{a} \tag{7}$$

with

$$\mathbf{a} = \sqrt{\mathbf{Z}_0}^{-1}\mathbf{v}_i \tag{8a}$$

$$\mathbf{b} = \sqrt{\mathbf{Z}_0}^{-1}\mathbf{v}_r \tag{8b}$$

$$\mathbf{S} = (\mathbf{I} + \sqrt{\mathbf{Z}_0}\mathbf{Y}\sqrt{\mathbf{Z}_0})^{-1}(\mathbf{I} - \sqrt{\mathbf{Z}_0}\mathbf{Y}\sqrt{\mathbf{Z}_0}). \tag{9}$$

It is noted that the scattering matrix $\mathbf{S}$ in (9) becomes identical to $\tilde{\mathbf{S}}$ in (6) when all ports are terminated by the same reference impedance. A diagonal element $\mathbf{S}_{jj}$ defines the reflected wave at port j due to an impinging (incident) wave on the same port while an offdiagonal element $\mathbf{S}_{ij}$ defines the reflected wave on port i due to an impinging wave on port j(i.e., the transmitted wave from port j to port i).

From (9), one can deduce a transformation from S-parameters to Y-parameters

$$\mathbf{Y} = \sqrt{\mathbf{Z}_0}^{-1}(\mathbf{I} - \mathbf{S})(\mathbf{I} + \mathbf{S})^{-1}\sqrt{\mathbf{Z}_0}^{-1}. \tag{10}$$

C. Transfer Function

A general transfer function $\mathbf{H}$ has n_1 inputs and n_2 outputs collected in vectors $\mathbf{u}$ and $\mathbf{y}$(11) where, in general, $n_1 \neq n_2$. Transfer functions are used for representing phenomena that do not directly interact with the main circuit over the ports

$$\mathbf{y} = \mathbf{H}\mathbf{u}. \tag{11}$$

III. System Modeling

A. Model Formulation

A rational model of $\mathbf{Y}$, $\mathbf{Z}$, $\mathbf{S}$ and $\mathbf{H}$ can be formulated in alternative ways. We assume that the extracted model is either on the pole-residue form (12) or the state-space form (13) where $\mathbf{F}$ denotes any of the four matrices $\mathbf{Y}$, $\mathbf{Z}$, $\mathbf{S}$, or $\mathbf{H}$ and s is frequency, $s = \sigma + j\omega$. The improper term $s\mathbf{E}$ in (12) and (13) is zero for the scattering case. The pole-residue model implies a common pole set for all elements of $\mathbf{F}$

$$\mathbf{F}(s) = \mathbf{R}_0 + \sum_{m=1}^{N} \frac{\mathbf{R}_m}{s - a_m} + s\mathbf{E} \tag{12}$$

$$\mathbf{F}(s) = \mathbf{D} + \mathbf{C}(s\mathbf{I} - \mathbf{A})^{-1}\mathbf{B} + s\mathbf{E}, \quad \mathbf{D} = \mathbf{R}_0. \tag{13}$$

In our examples, we will start from a model on pole-residue form (12). which we convert into the state-space form (13) as follows. Each term in the sum of (12) is subjected to the factorization

$$\mathbf{R}_m \frac{1}{s - a_m} = \mathbf{R}_m \left(\frac{1}{s - a_m}\mathbf{I}\right)\mathbf{I} \tag{14}$$

TABLE I
MATRIX DIMENSIONS OF THE STATE-SPACE MODEL

Matrix	**A**	**B**	**C**	**D**	**E**
Dimension	$n_1N\times n_1N$	$n_1N\times n_1$	$n_2\times n_1N$	$n_2\times n_1$	$n_2\times n_1$

TABLE II
PHYSICALITY CONSTRAINTS AND MATRIX DIMENSION.

Parameter	Y (or Z)	S	H
Symmetry	$\mathbf{Y}=\mathbf{Y}^T$	$\mathbf{S}=\mathbf{S}^T$	–
Realness	$\mathbf{Y}(s)=\mathbf{Y}^*(-s)$	$\mathbf{S}(s)=\mathbf{S}^*(-s)$	$\mathbf{H}(s)=\mathbf{H}^*(-s)$
Stability and causality	$\mathrm{Re}\{a_m\}<0$, $m=1\ldots N$	$\mathrm{Re}\{a_m\}<0$, $m=1\ldots N$	$\mathrm{Re}\{a_m\}<0$, $m=1\ldots N$
Passivity	$\lambda(\mathbf{Y}+\mathbf{Y}^H)<0$	$\sigma_{\max}<1$	–
Dimension	$(n\times n)$	$(n\times n)$	$(n_2\times n_1)$

which defines a state-space model with parameters

$$\mathbf{C}_m=\mathbf{R}_m,\quad \mathbf{A}_m=\frac{1}{a_m}\mathbf{I},\quad \mathbf{B}_m=\mathbf{I}. \tag{15}$$

By combining the state-space model from all terms in (13), we obtain the total state-space model which has a diagonal state matrix $\mathbf{A}$ and a sparse $\mathbf{B}$ of ones and zeros. The poles a_m, $m=1\ldots N$ are repeated in $\mathbf{A}$ as many times as there are columns in $\mathbf{F}$. For a model with n_1 inputs, n_2 outputs, and N pole-residue terms, the matrix dimensions become as shown in Table I. Further details about the conversion process are found in [22, App.]. The interfacing procedures developed in this paper are applicable also to general state-space models of the form (13) (i.e., models that do not originate from the pole-residue form (12)).

B. Physicality Constraints

The models (12) and (13) must be subjected to constraints during their extraction process in order to conform with physicality constraints pertaining to the respective models [15]. Table II lists the required constraints for the respective model parameter types as well as the resulting matrix dimensions. In the table, superscripts $*$ and H denote complex conjugate and Hermitian (complex conjugate and transpose), respectively. $\sigma_{\max}$ denotes maximum singular value of $\mathbf{S}$ over all frequencies. The physicality constraints for $\mathbf{Y}$ and $\mathbf{Z}$ are identical.

Since there are usually no symmetry constraints for a general transfer function, one may alternatively fit each column of $\mathbf{H}$ with a private pole set

$$\mathbf{H}=[\,\mathbf{h}_1\quad \mathbf{h}_2\quad \cdots\quad \mathbf{h}_{n1}\,],$$
$$\mathbf{h}_j(s)=\mathbf{r}_{0,j}+\sum_{m=1}^{N}\frac{\mathbf{r}_{m,j}}{s-a_{m,j}}+s\mathbf{e}_j. \tag{16}$$

This model (16) can again be cast in the form of a state-space model (13) with diagonal $\mathbf{A}$ and sparse $\mathbf{B}$, but without pole repetitions.

IV. DISCRETE CONVOLUTION

In the time domain, the state equation associated with $\mathbf{F}(s)$ in (13) is

$$\dot{\mathbf{x}}=\mathbf{A}\mathbf{x}+\mathbf{B}\mathbf{u} \tag{17a}$$
$$\mathbf{y}=\mathbf{C}\mathbf{x}+\mathbf{D}\mathbf{u}+\mathbf{E}\dot{\mathbf{u}}. \tag{17b}$$

We now wish to evaluate the output $\mathbf{y}$ of (17) from a general input $\mathbf{u}$ in a time-domain simulation based on a fixed time step length Δt (i.e., the discrete convolution between the input and the system impulse response $\mathbf{y}(t)=\mathbf{F}(t)^*\mathbf{u}(t)$).

A. Regular Part

First, consider the case with $\mathbf{E}=0$. Equation (17) is approximated with the central difference equation

$$\frac{\mathbf{x}_k-\mathbf{x}_{k-1}}{\Delta t}=\mathbf{A}\frac{\mathbf{x}_k+\mathbf{x}_{k-1}}{2}+\mathbf{B}\frac{\mathbf{u}_k+\mathbf{u}_{k-1}}{2} \tag{18a}$$
$$\mathbf{y}_k=\mathbf{C}\mathbf{x}_k+\mathbf{D}\mathbf{u}_k \tag{18b}$$

where k denotes the kth time step. Solving (18) for $\mathbf{x}_k$, we obtain

$$\mathbf{x}_k=\left(\mathbf{I}-\mathbf{A}\frac{\Delta t}{2}\right)^{-1}\times\left[\left(\mathbf{I}+\mathbf{A}\frac{\Delta t}{2}\right)\mathbf{x}_{k-1}+\frac{\Delta t}{2}\mathbf{B}(\mathbf{u}_k+\mathbf{u}_{k-1})\right] \tag{19a}$$
$$\mathbf{y}_k=\mathbf{C}\mathbf{x}_k+\mathbf{D}\mathbf{u}_k. \tag{19b}$$

Simplifying the notation gives

$$\mathbf{x}_k=\boldsymbol{\alpha}\mathbf{x}_{k-1}+\boldsymbol{\lambda}\mathbf{B}\mathbf{u}_k+\boldsymbol{\mu}\mathbf{B}\mathbf{u}_{k-1} \tag{20a}$$
$$\mathbf{y}_k=\mathbf{C}\mathbf{x}_k+\mathbf{D}\mathbf{u}_k \tag{20b}$$

with

$$\boldsymbol{\alpha}=\left(\mathbf{I}-\mathbf{A}\frac{\Delta t}{2}\right)^{-1}\left(\mathbf{I}+\mathbf{A}\frac{\Delta t}{2}\right) \tag{21a}$$
$$\boldsymbol{\lambda}=\boldsymbol{\mu}=\left(\mathbf{I}-\mathbf{A}\frac{\Delta t}{2}\right)^{-1}\frac{\Delta t}{2} \tag{21b}$$

where $\boldsymbol{\alpha}$, $\boldsymbol{\lambda}$, and $\boldsymbol{\mu}$ are diagonal matrices of the same dimension as $\mathbf{A}$ since $\mathbf{A}$ was assumed diagonal, and $\boldsymbol{\lambda}=\boldsymbol{\mu}$. The same result (20) would be obtained if one subjected the (17) to integration by the trapezoidal rule. We will accordingly refer to the recursive formula (20) as trapezoidal integration.

In (20a), $\mathbf{x}_k$ depends on the input $\mathbf{u}_k$ in the same time step. This simultaneous dependency is removed by introducing a change of variable

$$\mathbf{x}_k=\mathbf{x}'_k+\boldsymbol{\lambda}\mathbf{B}\mathbf{u}_k \tag{22}$$

which leads to a modification of (20) as follows:

$$\mathbf{x}'_k=\boldsymbol{\alpha}\mathbf{x}'_{k-1}+(\boldsymbol{\alpha}\boldsymbol{\lambda}+\boldsymbol{\mu})\mathbf{B}\mathbf{u}_{k-1} \tag{23a}$$
$$\mathbf{y}_k=\mathbf{C}\mathbf{x}'_k+(\mathbf{D}+\mathbf{C}\boldsymbol{\lambda}\mathbf{B})\mathbf{u}_k. \tag{23b}$$

By scaling the input and renaming the state variable to $\mathbf{x}$, we arrive at the final result

$$\mathbf{x}_k=\boldsymbol{\alpha}\mathbf{x}_{k-1}+\mathbf{B}\mathbf{u}_{k-1} \tag{24a}$$
$$\mathbf{y}_k=\tilde{\mathbf{C}}\mathbf{x}_k+\mathbf{G}\mathbf{u}_k \tag{24b}$$

where

$$\tilde{\mathbf{C}}=\mathbf{C}(\boldsymbol{\alpha}\boldsymbol{\lambda}+\boldsymbol{\mu}),\quad \mathbf{G}=(\mathbf{D}+\mathbf{C}\boldsymbol{\lambda}\mathbf{B}). \tag{25}$$

B. Irregular Part

Next, consider the contribution from a nonzero $\mathbf{E}$. In the time domain, we have

$$\mathbf{y} = \mathbf{E}\dot{\mathbf{u}}. \tag{26}$$

Application of trapezoidal integration gives

$$\frac{\mathbf{y}_k + \mathbf{y}_{k-1}}{2} = \mathbf{E}\frac{\mathbf{u}_k - \mathbf{u}_{k-1}}{\Delta t} \tag{27}$$

and so we can write

$$\mathbf{x}_k = -\mathbf{x}_{k-1} + \frac{2\mathbf{E}}{\Delta t}(\mathbf{u}_k - \mathbf{u}_{k-1}) \tag{28a}$$

$$\mathbf{y}_k = \mathbf{x}_k. \tag{28b}$$

The output $\mathbf{y}_k$ depends on the input $\mathbf{u}_k$ in the same time step. This simultaneous dependency is removed by introducing the transformed variable

$$\mathbf{x}'_k = \mathbf{x}_k + \frac{2\mathbf{E}}{\Delta t}\mathbf{u}_k. \tag{29}$$

Inserting (29) into (28) gives

$$\mathbf{x}'_k = -\mathbf{x}'_{k-1} - \frac{4\mathbf{E}}{\Delta t}\mathbf{u}_{k-1} \tag{30a}$$

$$\mathbf{y}_k = \mathbf{x}'_k + \frac{2\mathbf{E}}{\Delta t}\mathbf{u}_k. \tag{30b}$$

The recursive formula (30) is included in the ditto formula for the regular part (24) by augmenting matrices $\tilde{\mathbf{C}}$, $\boldsymbol{\alpha}$, $\mathbf{B}$, and $\mathbf{G}$ as follows:

$$\tilde{\mathbf{C}} \rightarrow [\,\tilde{\mathbf{C}} \quad \mathbf{I}\,], \quad \boldsymbol{\alpha} \rightarrow \begin{bmatrix} \boldsymbol{\alpha} & 0 \\ 0 & -\mathbf{I} \end{bmatrix}$$

$$\mathbf{B} \rightarrow \begin{bmatrix} \mathbf{B} \\ -\frac{4\mathbf{E}}{\Delta t} \end{bmatrix}, \quad \mathbf{G} \rightarrow \mathbf{G} + \frac{2\mathbf{E}}{\Delta t}. \tag{31}$$

V. Model Interface With Circuit Solver

A. Y-Parameters

In the Y-parameter case, the input $\mathbf{u}$ in (17) is voltage $\mathbf{v}$ and the response $\mathbf{y}$ is current $\mathbf{i}$. From (24), we obtain the recursive formula

$$\mathbf{x}_k = \boldsymbol{\alpha}\mathbf{x}_{k-1} + \mathbf{B}\mathbf{v}_{k-1} \tag{32a}$$

$$\mathbf{i}_k = \tilde{\mathbf{C}}\mathbf{x}_k + \mathbf{G}\mathbf{v}_k \tag{32b}$$

which is cast in the form of a Norton equivalent with current source

$$\mathbf{i}_{\mathrm{his},k} = -\tilde{\mathbf{C}}\mathbf{x}_k \tag{33}$$

with $\tilde{\mathbf{C}}$ and $\mathbf{G}_{\mathrm{Norton}} = \mathbf{G}$ given in (25).

B. Z-Parameters

In the Z-parameter case, the input $\mathbf{u}$ in (17) is current $\mathbf{i}$ and the response $\mathbf{y}$ is voltage $\mathbf{v}$. In (24), this gives

$$\mathbf{x}_k = \boldsymbol{\alpha}\mathbf{x}_{k-1} + \mathbf{B}\mathbf{i}_{k-1} \tag{34a}$$

$$\mathbf{v}_k = \tilde{\mathbf{C}}\mathbf{x}_k + \mathbf{G}\mathbf{i}_k \tag{34b}$$

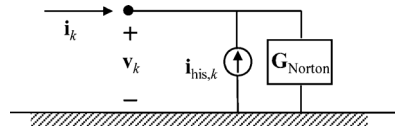

Fig. 3. Norton equivalent for (32).

which is written as a Thevenin equivalent with voltage source

$$\mathbf{v}_{\mathrm{his},k} = \tilde{\mathbf{C}}\mathbf{x}_k \tag{35}$$

with $\tilde{\mathbf{C}}$ and $\mathbf{Z}_{\mathrm{Thevenin}} = \mathbf{G}$ given in (25).

It is, however, convenient to transform the Thevenin equivalent into a Norton equivalent in order to eliminate the internal nodes

$$\mathbf{G}_{\mathrm{Norton}} = \mathbf{Z}_{\mathrm{Thevenin}}^{-1} \tag{36a}$$

$$\mathbf{i}_{\mathrm{his},k} = \mathbf{G}_{\mathrm{Norton}}\mathbf{v}_{\mathrm{his},k}. \tag{36b}$$

C. S-Parameters

From the relations $\mathbf{v} = \mathbf{v}_i + \mathbf{v}_\mathrm{r}$ (3), $\mathbf{a} = \sqrt{\mathbf{Z}_0}^{-1}\mathbf{v}_i$, $\mathbf{b} = \sqrt{\mathbf{Z}_0}^{-1}\mathbf{v}_r$ (8), and $\mathbf{b} = \mathbf{S}\mathbf{a}$ (7), we obtain the voltage by (37a). Similarly, via the relation between voltage waves and current by (5) $\mathbf{i} = \mathbf{Z}_0^{-1}(\mathbf{v}_i - \mathbf{v}_r)$, we obtain the current as

$$\mathbf{v} = \sqrt{\mathbf{Z}_0}(\mathbf{a} + \mathbf{b}) \tag{37a}$$

$$\mathbf{i} = \sqrt{\mathbf{Z}_0}^{-1}(\mathbf{a} - \mathbf{b}). \tag{37b}$$

For the convolution between $\mathbf{a}$ and $\mathbf{S}$ in the time domain, the input $\mathbf{u}$ in (17) is replaced with $\mathbf{a}$ and the response $\mathbf{y}$ is replaced by $\mathbf{b}$. This gives for the recursive formula (24)

$$\mathbf{x}_k = \boldsymbol{\alpha}\mathbf{x}_{k-1} + \mathbf{B}\mathbf{a}_{k-1} \tag{38a}$$

$$\mathbf{b}_k = \tilde{\mathbf{C}}\mathbf{x}_k + \mathbf{G}\mathbf{a}_k. \tag{38b}$$

Combining (38) with (37) gives

$$\mathbf{v}_k = \sqrt{\mathbf{Z}_0}\left[\tilde{\mathbf{C}}\mathbf{x}_k + (\mathbf{I} + \mathbf{G})\mathbf{a}_k\right] \tag{39a}$$

$$\mathbf{i}_k = \sqrt{\mathbf{Z}_0}^{-1}\left[-\tilde{\mathbf{C}}\mathbf{x}_k + (\mathbf{I} - \mathbf{G})\mathbf{a}_k\right]. \tag{39b}$$

Solving for $\mathbf{a}_k$ in (39a) and inserting in (39b) gives

$$\mathbf{i}_k = \sqrt{\mathbf{Z}_0}^{-1}[(\mathbf{I} - \mathbf{G})(\mathbf{I} + \mathbf{G})^{-1}]\sqrt{\mathbf{Z}_0}^{-1}\mathbf{v}_k - 2\sqrt{\mathbf{Z}_0}^{-1}(\mathbf{I} + \mathbf{G})^{-1}\tilde{\mathbf{C}}\mathbf{x}_k. \tag{40}$$

This defines the Norton equivalent in Fig. 3 with

$$\mathbf{G}_{\mathrm{Norton}} = \sqrt{\mathbf{Z}_0}^{-1}[(\mathbf{I} - \mathbf{G})(\mathbf{I} + \mathbf{G})^{-1}]\sqrt{\mathbf{Z}_0}^{-1} \tag{41a}$$

$$\mathbf{i}_{\mathrm{his},k} = 2\sqrt{\mathbf{Z}_0}^{-1}(\mathbf{I} + \mathbf{G})^{-1}\tilde{\mathbf{C}}\mathbf{x}_k = \boldsymbol{\Gamma}\mathbf{x}_k. \tag{41b}$$

The state variable $\mathbf{x}_k$ is obtained from (38a) which has $\mathbf{a}_{k-1}$ as the stimulus. The incident wave $\mathbf{a}_{k-1}$ is calculated via the voltage $\mathbf{v}_{k-1}$ and (37a) as follows:

$$\mathbf{v}_{k-1} = \sqrt{\mathbf{Z}_0}(\mathbf{a}_{k-1} + \mathbf{b}_{k-1}) = \sqrt{\mathbf{Z}_0}(\mathbf{a}_{k-1} + \tilde{\mathbf{C}}\mathbf{x}_{k-1} + \mathbf{G}\mathbf{a}_{k-1}). \tag{42}$$

TABLE III
PROCEDURE FOR UPDATING THE HISTORY CURRENT SOURCE.

Step 1	Calculate $\mathbf{a}_{k-1}$ by (43)
Step 2	Calculate $\mathbf{x}_k$ by (38a)
Step 3	Calculate $\mathbf{i}_{\text{his},k}$ by (41b)

Solving (42) gives $\mathbf{a}_{k-1}$ as

$$\mathbf{a}_{k-1} = (\mathbf{I}+\mathbf{G})^{-1}(\sqrt{\mathbf{Z}_0}^{-1}\mathbf{v}_{k-1} - \tilde{\mathbf{C}}\mathbf{x}_{k-1}). \quad (43)$$

The procedure for updating the current source is summarized in Table III.

D. Transfer Function

The transfer function case is handled directly by (24) without a Norton interface with the electrical circuit since the transfer function does, per assumption, not interfere with the electrical circuit over its ports. The input $\mathbf{u}$ can represent any quantity (e.g., voltage or current). The output $\mathbf{y}$ can be further processed (e.g., in a control system) or it could be used for controlling ideal sources in the simulation. The latter case gives a one-time step delay in the response.

VI. COMPUTATIONAL CONSIDERATIONS

A. Pole-Residue Modeling

We usually prefer to develop rational models on the pole-residue form (12) since this is the model type that is naturally produced by vector fitting (VF) [8]. When converting a pole-residue model into state-space form (13), one obtains a model where $\mathbf{A}$ is diagonal and $\mathbf{B}$ is sparse matrix of ones and zeros (15). These properties are utilized for increasing the computational speed of the time-domain simulation as follows.

1) The diagonal form of $\mathbf{A}$ is utilized when updating the state variable in (24a), (34a), and (38a). Each element j of the matrix-vector product $\boldsymbol{\alpha}\mathbf{x}_k$ is obtained as $(\boldsymbol{\alpha}\mathbf{x}_k)(j) = \boldsymbol{\alpha}(j,j)\mathbf{x}_k(j)$.
2) The sparse $\mathbf{B}$ matrix has a single one in each row. $\mathbf{B}$ is therefore a selector matrix which associates each element u_i of the input $\mathbf{u}$ with row partitions $\mathbf{A}_i$ and $\mathbf{x}_{ki}$. Accordingly, there is no need for formally multiplying $\mathbf{B}$ with $\mathbf{x}_k$.
3) Complex elements in $\mathbf{x}_k$ occur in conjugate pairs. In each pair, the two terms give a contribution to the history source $\mathbf{i}_{\text{his},k}$ whose real parts are equal [5]. To see this, consider a complex conjugate pair

$$h(s) = \frac{r'+jr''}{s-(a'+ja'')} + \frac{r'-jr''}{s-(a'-ja'')}. \quad (44)$$

The time-domain impulse response is

$$h(t) = (r'+jr'')e^{(a'+ja'')t} + (r'-jr'')e^{(a'-ja'')t}. \quad (45)$$

$h(t)$ can be rewritten as $h(t) = h_1(t) + h_2(t)$ where

$$\begin{aligned} h_1(t) &= r'e^{a't}(e^{ja''t} + e^{-ja''t}) \\ &= 2r'e^{a't}\cos(a''t) \end{aligned} \quad (46a)$$

$$\begin{aligned} h_2(t) &= jr''e^{a't}(e^{ja''t} - e^{-ja''t}) \\ &= -2r''e^{a't}\sin(a''t). \end{aligned} \quad (46b)$$

If one deletes the second term in (44), we now obtain for (46)

$$\begin{aligned} \tilde{h}_1(t) &= r'e^{a't}e^{ja''t} \\ &= r'e^{a't}(\cos(a''t) + j\sin(a''t)) \end{aligned} \quad (47a)$$

$$\begin{aligned} \tilde{h}_2(t) &= jr''e^{a't}e^{ja''t} \\ &= jr''e^{a't}(\cos(a''t) + j\sin(a''t)). \end{aligned} \quad (47b)$$

Retaining only the real part of (47) gives

$$\text{Re}\{\tilde{h}_1(t)\} = r'e^{a't}\cos(a''t) = \frac{1}{2}h_1(t) \quad (48a)$$

$$\text{Re}\{\tilde{h}_2(t)\} = -r''e^{a't}\sin(a''t) = \frac{1}{2}h_2(t). \quad (48b)$$

Therefore, deleting the second term in (44) has the effect of reducing the real part of $h(t)$ by a factor of two. This allows us to utilize only one of the two terms in (44) and scale the output of the convolution (i.e., $\mathbf{i}_{\text{his},k}$) with a factor of two and discard its imaginary part. This gives nearly a 50% reduction in computation time for models with mainly complex poles.

4) An alternative way of increasing computational efficiency when handling complex poles is to convert the model into a real-only model. This gives a model with 2×2 blocks on the diagonal of $\mathbf{A}$ [23]

$$\begin{aligned} \hat{\mathbf{A}} &= \begin{bmatrix} \text{Re}\{a\} & \text{Im}\{a\} \\ -\text{Im}\{a\} & \text{Re}\{a\} \end{bmatrix} \\ \hat{\mathbf{c}} &= [\,\text{Re}\{\mathbf{c}\} \quad \text{Im}\{\mathbf{c}\}\,] \end{aligned} \quad (49a)$$

$$\hat{\mathbf{b}} = \begin{bmatrix} 2\text{Re}\{\mathbf{b}^T\} \\ -2\text{Im}\{\mathbf{b}^T\} \end{bmatrix} = \begin{bmatrix} 2\text{Re}\{\mathbf{b}^T\} \\ 0 \end{bmatrix}. \quad (49b)$$

B. State-Space Modeling

If the starting point is a general state-space model, one may diagonalize the model. This gives a diagonal $\mathbf{A}$ and so $\boldsymbol{\alpha}\mathbf{x}_k$ can be computed as in the pole-residue case. However, the $\mathbf{B}$-matrix will now, in general, be full. In the case of a sparse state-space model, one may alternatively use sparse computations.

VII. INTERFACE WITH EMTP-TYPE SOLVERS

All major EMTP-type simulation tools are based on Dommel's method [16], where each dynamic element is represented by its Norton equivalent of a fixed conductance matrix in parallel with a history current source. This applies to all (linear) dynamic elements, such as RLC branches and transmission lines. Typically, one will have a separate subroutine for each model type. At the first time step ($t = 0$), each subroutine initializes its model by calculating the model's coefficients (which are dependent on Δt) and its conductance matrix which is added to the global system conductance matrix. In all subsequent time steps, the history current sources are updated based on the model's terminal voltages. The process is outlined in Fig. 5. The current $\boldsymbol{i}_k$ is the global current vector; it

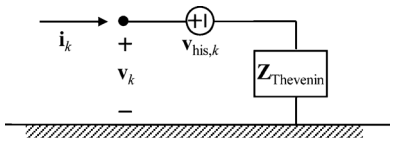

Fig. 4. Thevenin equivalent for (26).

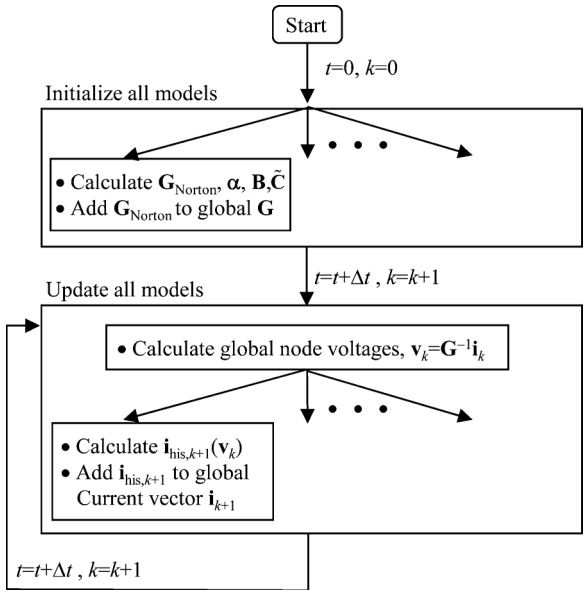

Fig. 5. Time-domain simulation.

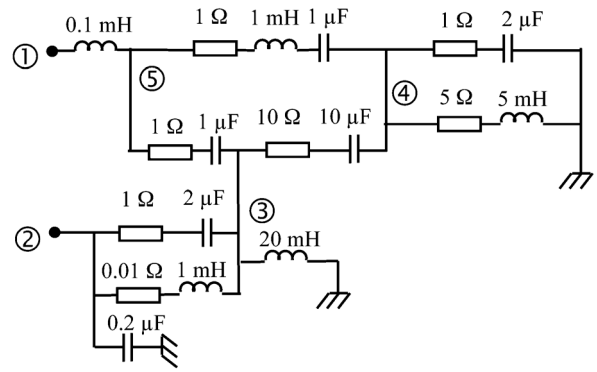

Fig. 6. Two-port circuit.

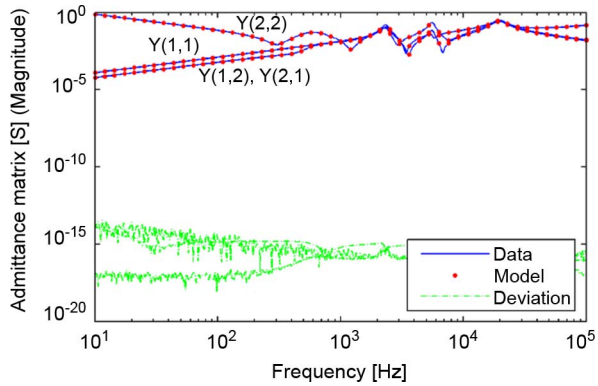

Fig. 7. Fitted Y-parameters (magnitude).

is the sum of the independent current sources and the history current sources.

In the following sections, we show a number of example simulations using a small EMTP-type simulation program implemented in Matlab. The Matlab implementation has later been converted into standard components for the PSCAD-EMTDC simulation environment with final testing almost complete at the time of writing.

VIII. Example: Electrical Circuit

In the following text, we demonstrate the alternative model interfacing approaches for a small two-port electrical circuit. First, we calculate the port characteristics defined by Y-, Z-, and S-parameters. Next, we fit a rational model to each of these parameter sets with the correct model order such that the fitting error is negligible. Finally, the three models are interfaced with an EMTP-type simulation program and employed in a transient simulation. The simulation results by the three alternative approaches are compared with that obtained using a detailed representation of the original RLC circuit. We also demonstrate the use of the transfer function for computing an internal voltage in the system.

A. Circuit Layout and Port Characteristics

Fig. 6 shows a small electrical circuit with two external ports, numbered 1 and 2. The objective is to represent the circuit with a rational model with respect to these two ports.

Using the nodal admittance approach, the 5×5 admittance matrix is calculated for the system as a discrete function of frequency and is reduced to a 2×2 matrix $\mathbf{Y}$ with respect to the two external ports 1 and 2. The impedance matrix $\mathbf{Z}$ is computed as the matrix inverse $\mathbf{Z} = \mathbf{Y}^{-1}$. The scattering matrix $\mathbf{S}$ is computed from $\mathbf{Y}$ by (9), assuming different reference resistors for ports 1 and 2

$$\mathbf{Z}_0 = \begin{bmatrix} 100 & 0 \\ 0 & 200 \end{bmatrix}. \tag{50}$$

In order to demonstrate the application of the transfer function $\mathbf{H}$, we also compute the voltage transfer from port 1 to port 2 $v_2 = Hv_1$, $H = -Y_{21}/Y_{22}$.

B. Pole-Residue Modeling

The port characteristics were computed using 501 logarithmically spaced frequency samples between 10 Hz and 100 kHz. A 10th-order pole-residue model (12) was fitted to each of the given parameter sets $\mathbf{Y}(2 \times 2)$, $\mathbf{Z}(2 \times 2)$, and an 11th-order model to $\mathbf{S}(2 \times 2)$ and $H(1 \times 1)$. All models include a nonzero term $\mathbf{R}_0$ while $s\mathbf{E}$ is included only in the modeling of Y- and Z-parameters. We used VF [8] with relaxation [9] (for faster convergence) and sparse implementation [10] (for faster computations). Figs. 7–10 show the result from rational modeling. It is observed that all matrix elements have been accurately fitted since the magnitude of the (complex) deviation is very small.

C. Time-Domain Simulation

We next apply the four extracted models in an EMTP-type time-domain simulation using the interfacing approaches de-

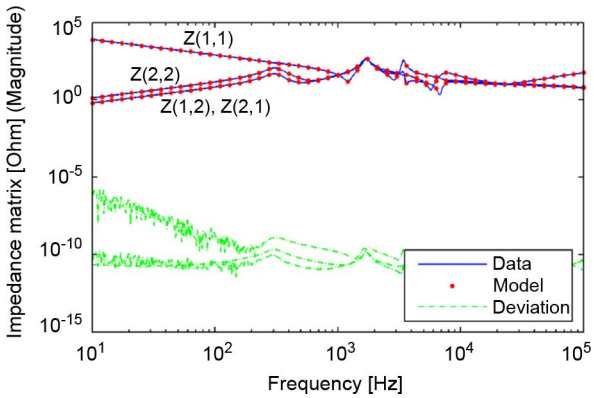

Fig. 8. Fitted Z-parameters (magnitude).

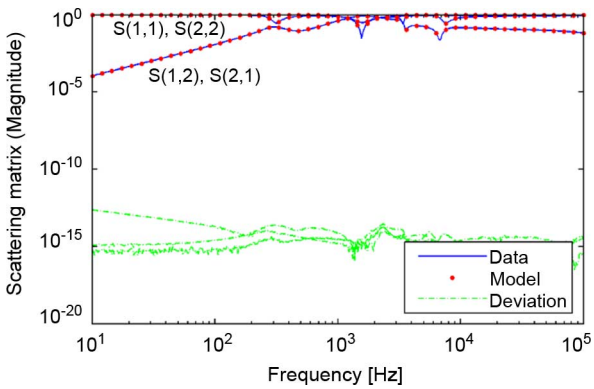

Fig. 9. Fitted S-parameters (magnitude).

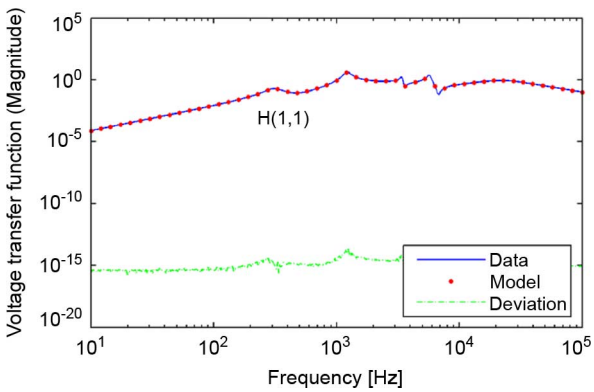

Fig. 10. Fitted voltage transfer function from port #1 to port #2 (magnitude).

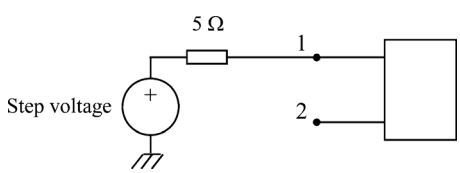

Fig. 11. Voltage excitation voltage at port #1.

scribed in Section V with trapezoidal integration. A unit step voltage behind a 5-Ω resistor is applied to port #1 with port #2 open. (See Fig. 11.) We simulate the current response at port #1 and the voltage response at port #2 with a $\Delta t = 10$-μs time step length. As a reference, we also perform a conventional lumped circuit simulation with trapezoidal integration using PSCAD.

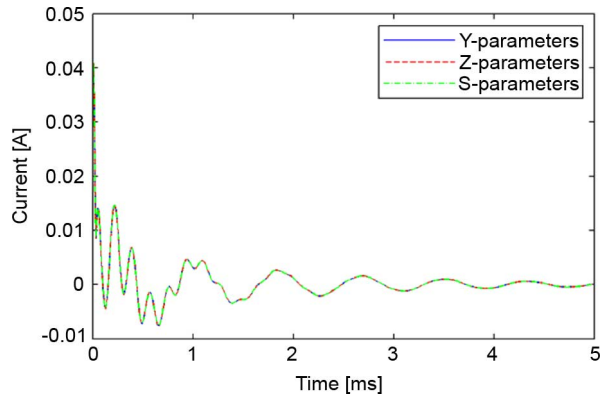

Fig. 12. Current response at port #1.

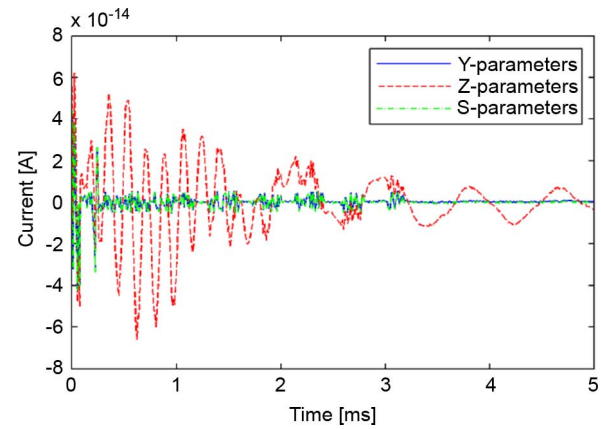

Fig. 13. Deviation from the current obtained from simulation by the lumped circuit.

Fig. 12 shows the simulated current response at terminal 1 when simulated via Y-, Z-, or S-parameters. As expected, the responses are virtually identical since the frequency-domain fitting errors are close to zero. Fig. 13 shows the deviation of the responses in Fig. 12 with that of the conventional lumped circuit simulation. The deviation is smaller than $1E-13$ and so the results are deemed identical.

Fig. 14 shows the simulated voltage at port #2 when simulated via Y-, Z-, or S-parameters. In addition, we have simulated this voltage via the voltage transfer from port #1 to port #2, when taking the voltage at port 1 (obtained from the Y-parameter model) as a known quantity. Again, all responses are virtually identical. This result is highlighted in Fig. 15 which shows the deviation from the conventional lumped circuit simulation. The deviation is smaller than $2E-12$.

IX. Example: Subnetwork Modeling From Computed Admittance Parameters

One application of the Y-parameter interfacing capability is the interfacing of a frequency-dependent network equivalent of a subnetwork. Fig. 16 shows a 345-kV, 27-bus system network which includes 22 transmission lines with a maximum length up to 200 km. A detailed model of this system is available in an EMTP-type simulation tool with transmission lines represented by traveling-wave models and loads represented by shunt elements at load buses (resistors, capacitors, and inductors). The

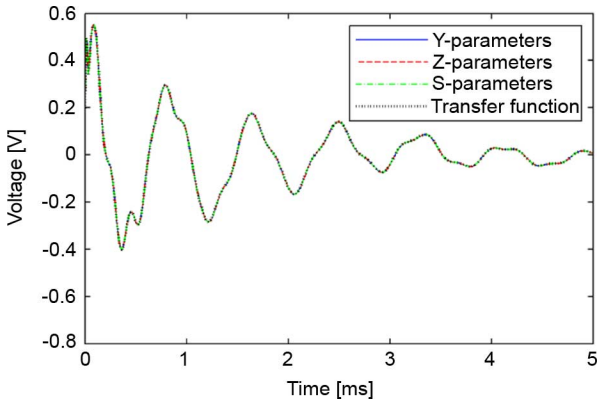

Fig. 14. Voltage response at port #2.

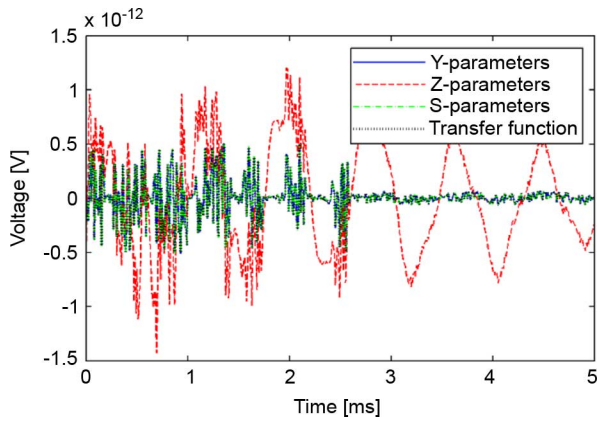

Fig. 15. Deviation from voltage obtained from simulation by the lumped circuit.

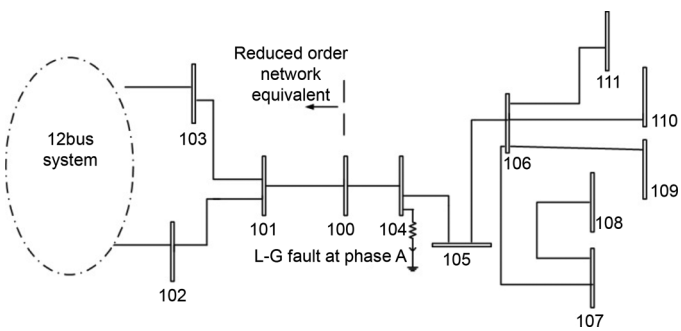

Fig. 16. Power system network.

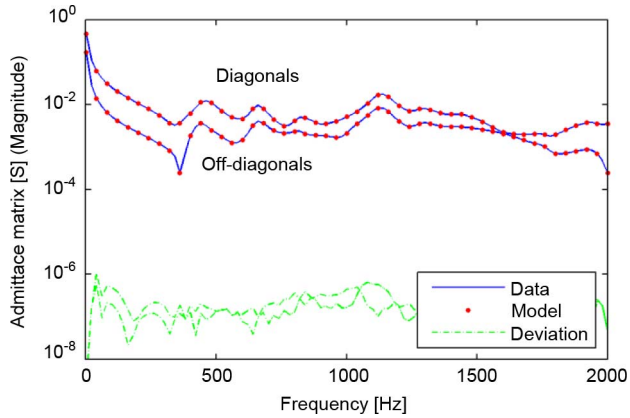

Fig. 17. Actual and fitted admittance matrices.

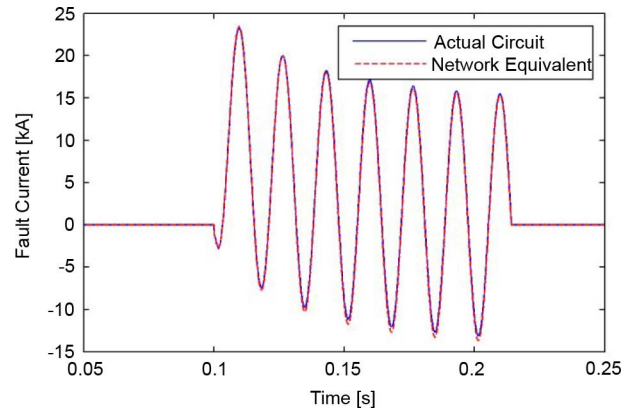

Fig. 18. Phase A fault current at bus 104.

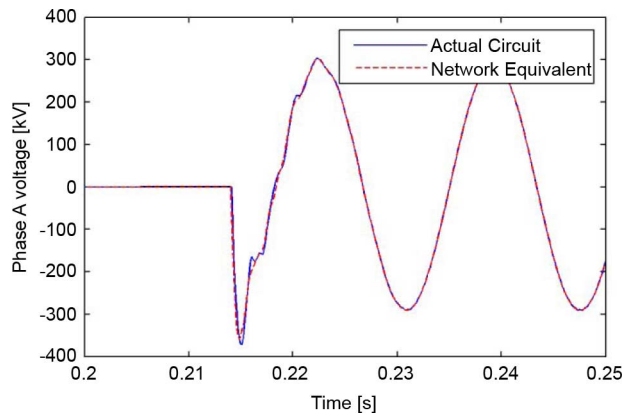

Fig. 19. Phase voltages at bus 104.

admittance response for the network as seen from bus #100 is obtained by performing a frequency scan at frequencies linearly distributed between 1 Hz and to 2 kHz in 20-Hz steps. Next, the network as seen from bus 100 is replaced by a reduced order network equivalent by fitting the admittance matrix by a pole-residue model (12) via VF [8]–[10]. Fig. 17 shows the elements of the actual and approximated admittance matrix as a function of frequency. The model is interfaced to the circuit solver using the procedure described in Section V-A. Current sources are added to the terminals of the network equivalent in order to maintain the correct steady-state power flow and voltages at each bus.

A line-to-ground fault is applied at bus #104 at $t = 0.10$ s, and the fault is cleared after $t = 0.21$ s. The fault current and voltage waveforms are shown in Figs. 18 and 19 with $\Delta t = 50\ \mu$s . It is observed that the network model reproduces the waveforms of the original, detailed model, although the model's upper frequency limit of 2 kHz prevents accurate reproduction of high-frequency components.

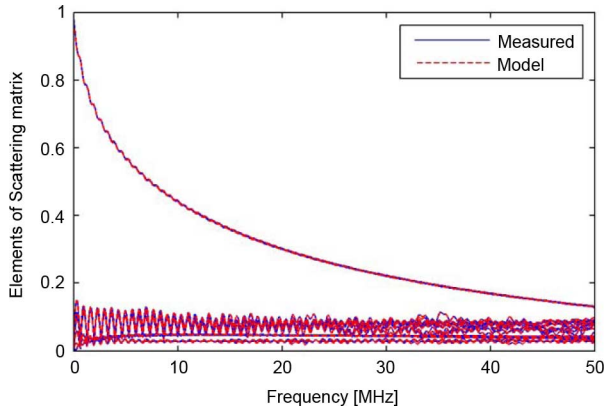

Fig. 20. Measured and fitted S-parameters.

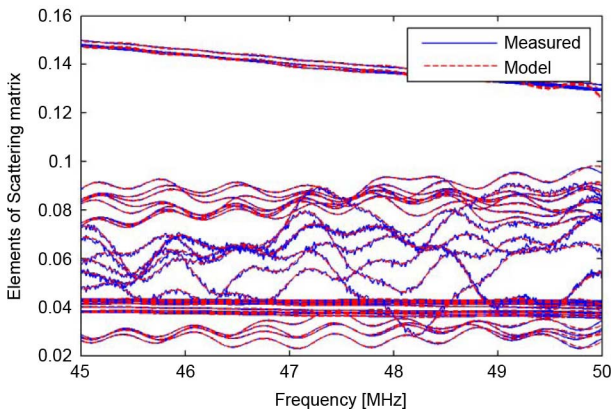

Fig. 21. Measured and fitted S-parameters (expanded view).

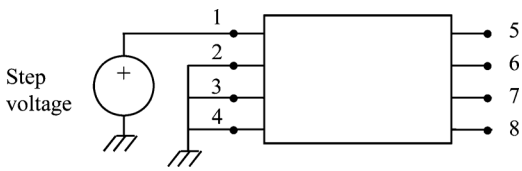

Fig. 22. Unit step voltage excitation.

X. Example: Cable Modeling From Measured Scattering Parameters

A 150-m four-conductor industrial cable has been characterized by S-parameter measurements between 9 kHz and 50 MHz in [25], with $Z_0 = 50\text{-}\Omega$ reference impedance. We calculate a pole-residue model (12) of the 8×8 $\mathbf{S}$ with $N = 200$ terms using VF [8]–[10] and subject it to passivity enforcement via residue matrix spectral perturbation [13]. Figs. 20 and 21 compare the measured and fitted S-parameters.

The pole-residue model is interfaced with an EMTP-type simulation program using the procedure in Section V-C. Conductor #1 is subjected to a unit step voltage excitation with the other conductors grounded at this end. (See Fig. 22.) All conductors are open at the receiving end.

Figs. 23 and 24 show, respectively, the simulated receiving end voltages and sending end currents with $\Delta t = 0.01$ μs. The simulation result is verified as follows. Using the rational model, samples $\mathbf{S}(\sigma + j\omega)$ are computed (in the complex plane)

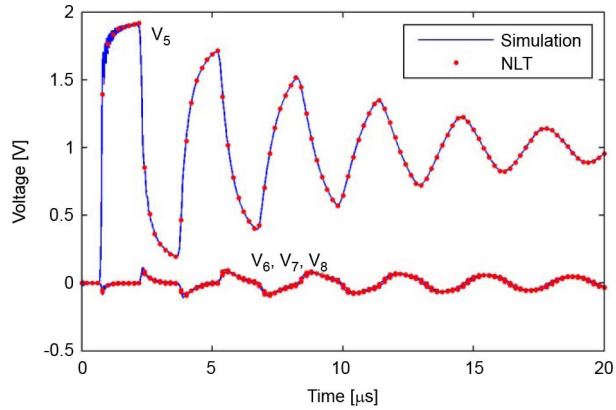

Fig. 23. Receiving-end voltages.

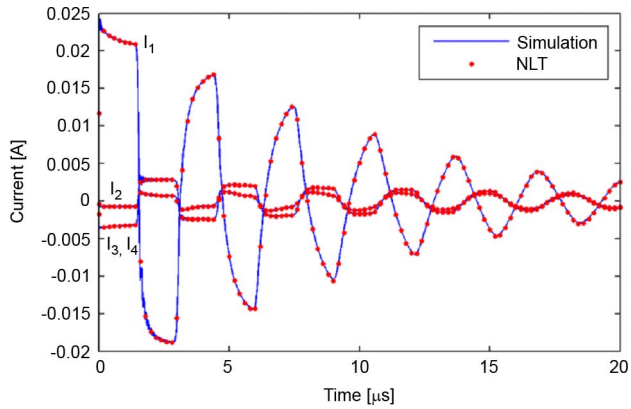

Fig. 24. Sending-end currents.

and converted into admittance samples $\mathbf{Y}(\sigma + j\omega)$ by (10). From $\mathbf{Y}$ and the nodal analysis method, the step response frequency-domain solution is computed for the voltages and currents which are transformed into the time domain using the Numerical Laplace transform (NLT) [26], [27], with the implementation described in [28]. The result is shown in Figs. 23 and 24. The solution by NLT is seen to agree closely with that of the simulation, thereby validating the model interfacing method.

XI. Discussion

The reader may wonder whether it is really necessary to have separate interfacing possibilities for alternative parameter sets (Y-, Z-, S-, transfer functions) since it possible to convert one parameter set into another set via formulae. By this reasoning, the Y-parameter interface should suffice for representing also the Z- and S-parameter sets. However, since the modeling of a given parameter set will, in practice, involve some level of inaccuracy, the model fidelity will depend on which parameter set it was extracted from. For instance, a rational model extracted from Y-parameters tends to be more accurate with low-impedance terminations than with high-impedance terminations while the situation is the opposite for a model extracted from Z-parameters. Also, one may in situations with measured parameters experience large error magnifications when converting from one parameter set to a different one. It is therefore advantageous to freely choose which parameter set the modeling should be based on.

The Matlab code used for model extraction and time-domain simulation in Section VIII (electrical circuit) can be freely downloaded from http://www.energy.sintef.no/Produkt/VECTFIT/index.asp.

XII. Conclusion

This paper addresses the task of interfacing a multiport rational model with EMTP-type circuit solvers via a Norton equivalent and convolution. We have shown how to do this for models that represent admittance (Y-) parameters, impedance (Z-) parameters, scattering (S-) parameters, and pure transfer functions which do not directly interact with the power system.

1) The details of implementation were shown for both pole-residue models and general state-space models, assuming a fixed time step and trapezoidal integration.
2) Comparison with a lumped circuit simulation showed that all model interfaces give exactly the same result independent on which parameter set they are based on, provided that the model extraction step was accurate.
3) The Y-parameter interface was demonstrated for use with subnetwork modeling of a 12-bus system. It was shown that the model could represent the transient behavior with adequate accuracy.
4) The S-parameter interface was demonstrated for the modeling of an industrial cable from S-parameter measurements. The interface was shown to accurately represent the information given in the S-parameter rational model.
5) Use of the alternative model's interfaces avoids the need for conversion between parameter sets, thereby avoiding potential deterioration of the model's accuracy.

Acknowledgment

The authors would like to thank B. Wunsch and his colleagues at ABB Switzerland Ltd, Corporate Research for providing us with the S-parameter data set in Section X.

References

[1] A. Morched, L. Marti, and J. Ottevangers, "A high frequency transformer model for the EMTP," *IEEE Trans. Power Del.*, vol. 8, no. 3, pp. 1615 –1626, Jul. 1993.
[2] B. Gustavsen, "Wide band modeling of power transformers," *IEEE Trans. Power Del.*, vol. 19, no. 1, pp. 414–422, Jan. 2004.
[3] A. Morched, J. Ottevangers, and L. Marti, "Multi-port frequency dependent network equivalents for the EMTP," *IEEE Trans. Power Del.*, vol. 8, no. 3, pp. 1402–1412, Jul. 1993.
[4] M. Abdel-Rahman, R. Iravani, and A. Semlyen, "Two-layer network equivalent for electromagnetic transients," *IEEE Trans. Power Del.*, vol. 18, no. 4, pp. 1328–1335, Oct. 2003.
[5] T. Noda, "Identification of a multiphase network equivalent for electromagnetic transient calculations using partitioned frequency response," *IEEE Trans. Power Del.*, vol. 20, no. 2, pt. 1, pp. 1134–1142, Apr. 2005.
[6] Y. Liang, X. Lin, A. M. Gole, and M. Ming Yu, "Improved coherency-based wide-band equivalents for real-time digital simulators," *IEEE Trans. Power Syst.*, vol. 26, no. 3, pp. 1410–1417, Aug. 2011.
[7] U. D. Annakkage *et al.*, "Dynamic system equivalents: A survey of available techniques," *IEEE Trans. Power Del.*, vol. 27, no. 1, pp. 411–420, Jan. 2012.
[8] B. Gustavsen and A. Semlyen, "Rational approximation of frequency domain responses by vector fitting," *IEEE Trans. Power Del.*, vol. 14, no. 3, pp. 1052–1061, Jul. 1999.
[9] B. Gustavsen, "Improving the pole relocating properties of vector fitting," *IEEE Trans. Power Del.*, vol. 21, no. 3, pp. 1587–1592, Jul. 2006.
[10] D. Deschrijver, M. Mrozowski, T. Dhaene, and D. De Zutter, "Macromodeling of multiport systems using a fast implementation of the vector fitting method," *IEEE Microw. Wireless Compon. Lett.*, vol. 18, no. 6, pp. 383–385, Jun. 2008.
[11] B. Gustavsen and A. Semlyen, "Enforcing passivity for admittance matrices approximated by rational functions," *IEEE Trans. Power Syst.*, vol. 16, no. 1, pp. 97–104, Feb. 2001.
[12] S. Grivet-Talocia, "Passivity enforcement via perturbation of hamiltonian matrices," *IEEE Trans. Circuits Syst. I, Reg. Papers*, vol. 51, no. 9, pp. 1755–1769, Sep. 2004.
[13] B. Gustavsen, "Fast passivity enforcement for S-parameter models by perturbation of residue matrix eigenvalues," *IEEE Trans. Adv. Packag.*, vol. 33, no. 1, pp. 257–265, Feb. 2010.
[14] T. Dhaene, D. Deschrijver, and N. Stevens, "Efficient algorithm for passivity enforcement of S-parameter-based macromodels," *IEEE Trans. Microw. Theory Tech.*, vol. 57, no. 2, pp. 415–420, Feb. 2009.
[15] P. Triverio, S. Grivet-Talocia, M. S. Nakhla, and F. G. Canavero, *Stability, Causality, and Passivity in Electreical Interconnect Models*, vol. 30, no. 4, pp. 795–808, Nov. 2007.
[16] H. W. Dommel, *ElectroMagnetic Transients Program. Reference Manual (EMTP Theory Book)*. Portland, OR: Bonneville Power Administration, 1986.
[17] B. Gustavsen, "Computer code for rational approximation of frequency dependent admittance matrices," *IEEE Trans. Power Del.*, vol. 17, no. 4, pp. 1093–1098, Oct. 2002.
[18] B. Gustavsen and O. Mo, "Interfacing convolution based linear models to an electromagnetic transients program," in *Proc. Int. Conf. Power Syst. Transients*, Lyon, France, Jun. 4–7, 2007, p. 6.
[19] C. Dufour, J. Mahseredjian, and J. Belanger, "A combined state-space nodal method for the simulation of power system transients," *IEEE Trans. Power Del.*, vol. 26, no. 2, pp. 928–935, Apr. 2011.
[20] K. Kurokawa, "Power waves and the scattering matrix," *IEEE Trans. Microw. Theory Tech.*, vol. MTT-13, no. 2, pp. 194–202, Mar. 1965.
[21] Z. Zhongyuan, L. Fangcheng, and L. Guishu, "A high-frequency circuit model of a potential transformer for the very fast transient simulation in GIS," *IEEE Trans. Power Del.*, vol. 23, no. 4, pp. 1995–1999, Oct. 2008.
[22] A. Semlyen and B. Gustavsen, "A half-size singularity test matrix for fast and reliable passivity assessment of rational models," *IEEE Trans. Power Del.*, vol. 24, no. 1, pp. 345–351, Jan. 2009.
[23] E.-P. Li, E.-X. Liu, L. W. Li, and M.-S. Leong, "A coupled efficient and systematic full-wave time-domain macromodeling and circuit simulation method for signal integrity analysis of high-speed interconnects," *IEEE Trans. Adv. Packag.*, vol. 27, no. 1, pp. 213–223, Feb. 2004.
[24] A. Semlyen and A. Dabuleanu, "Fast and accurate switching transient calculations on transmission lines with ground return using recursive convolutions," *IEEE Trans. Power App. Syst.*, vol. 94, no. 2, pt. 1, pp. 561–571, Mar./Apr. 1975.
[25] S. Skibin, B. Wunsch, I. Stevanovic, and B. Gustavsen, "High-frequency cable models for system level simulations in power electronics applications," presented at the EMC Eur., Rome, Italy, Sep. 17–21, 2012.
[26] D. J. Wilcox, "Numerical Laplace transformation and inversion," *Int. J. Elect. Eng. Educ.*, vol. 15, pp. 247–265, 1978.
[27] L. M. Wedepohl, "Power system transients: Errors incurred in the numerical inversion of the Laplace transform," in *Proc. 26th Midwest Symp. Circuits Syst.*, Aug. 1983, pp. 174–178.
[28] P. Moreno and A. Ramirez, "Implementation of the numerical Laplace transform: A review task force on frequency domain methods for EMT studies," *IEEE Trans. Power Del.*, vol. 23, no. 4, pp. 2599–2609, Oct. 2008.
[29] A. C. S. Lima, B. Gustavsen, and A. B. Fernandes, "Inaccuracies in fitted frequency dependent networks due to finite precision of RLC branches," in *Proc. Int. Conf. Power Syst. Transients (IPST)*, Lyon, France, Jun. 2007, p. 5.

Bjørn Gustavsen (M'94–SM'03) was born in Norway in 1965. He received the M.Sc. and Dr.Ing. degrees in electrical engineering from the Norwegian Institute of Technology (NTH), Trondheim, Norway, in 1989 and 1993, respectively.

Since 1994, he has been a Chief Research Scientist at SINTEF Energy Research, Trondheim. He spent 1996 as a Visiting Researcher at the University of Toronto, Toronto, ON, Canada, and in 1998, he was with the Manitoba HVDC Research Centre, Winnipeg, MB, Canada. He was a Marie Curie Fellow at

the University of Stuttgart, Stuttgart, Germany, from 2001 to 2002. His interests include the simulation of electromagnetic transients and modeling of frequency-dependent effects.

H. M. Jeewantha De Silva was born in Ambalangoda, Sri Lanka. He received the B.Sc (Eng.) degree in electrical engineering from the University of Moratuwa, Sri Lanka, in 2001 and the Ph.D. degree in electrical engineering from the University of Manitoba, Winnipeg, MB, Canada, in 2009.

Currently, he is a Power System Simulation and Research Engineer at Manitoba Hydro International, Winnipeg. His interests are time-domain modeling of multiconductor underground cables and passivity enforcement of transmission lines.